Geophysical Research Letters

RESEARCH LETTER
10.1029/2025GL120398

Key Points:

- We develop a coherence-based power metric to detect and estimate the power of clustered foreshocks along the San Jacinto fault zone
- We find that 19 $M \geq 2.5$ events are preceded by 5 to 20-s-long foreshock sequences, dominantly along the base of the seismogenic zone
- Clustered foreshocks show a moment-rate power buildup, which might reflect accelerating aseismic slip or a growing cascade of ruptures

Supporting Information:

Supporting Information may be found in the online version of this article.

Correspondence to:

H. Huang,
hui_huang@tongji.edu.cn

Citation:

Huang, H., & Hawthorne, J. C. (2026). 19 clustered foreshock sequences along the San Jacinto fault zone: Possible role of frictional heterogeneity in extended earthquake nucleation. *Geophysical Research Letters*, *53*, e2025GL120398. https://doi.org/10.1029/2025GL120398

Received 4 NOV 2025
Accepted 31 MAR 2026

19 Clustered Foreshock Sequences Along the San Jacinto Fault Zone: Possible Role of Frictional Heterogeneity in Extended Earthquake Nucleation

Hui Huang[1] **and Jessica C. Hawthorne**[2]

[1]State Key Laboratory of Marine Geology, Tongji University, Shanghai, China, [2]Department of Earth Sciences, University of Oxford, Oxford, UK

Abstract Laboratory experiments and theoretical models suggest that earthquakes are preceded by extended nucleation phases, perhaps by slow but accelerating slip. However, such nucleation phases are hard to observe before natural earthquakes. Here we identify clustered foreshock sequences that could be nucleation signatures. We develop a coherence-based power metric to detect foreshock sequences along the San Jacinto fault zone (SJFZ) and then track the temporal evolution of foreshocks' moment-rate power. The results show that a small but significant fraction of $M \geq 2.5$ earthquakes (19 out of 681) are preceded by 5 to 20-s-long clustered foreshock sequences, which may reflect extended nucleation phases. The sequences preferentially occur near the base of the seismogenic zone, which likely contains frictionally heterogeneous patches of varying sizes. We identify a build-up of 2-8-Hz moment-rate power during the sequences and consider some interpretations: that the growing power reflects accelerating aseismic slip or growing cascades of ruptures.

Plain Language Summary Earthquake initiation in nature is still a mystery, although lab experiments or theoretical models suggest that there is a nucleation phase of slow but accelerating slip before the earthquake rupture begins. Foreshocks are widely used to probe the nucleation process, but the connection between foreshocks and the mainshock nucleation is still uncertain. Here we study earthquake nucleation along the SJFZ, where abundant seismicity and good station coverage make it an ideal site. Specifically, we detect extended and clustered foreshock sequences around the mainshock hypocenter which may indicate extended earthquake nucleation. We track the temporal evolution of foreshocks' source power by using a new coherence based power metric. Our results show that 19 clustered foreshock sequences occur near the base of the seismogenic zone. These observations are rare, but might indicate that prolonged earthquake nucleations occur under some fault conditions. We discuss possible rupture scenarios under conditions of frictional heterogeneity that lead to our observations. We observe growth of source power during foreshocks, which might reflect accelerating aseismic slip or growing cascades of ruptures. Our results provide new constraints on the fault condition control of earthquake nucleation behaviors along the SJFZ.

1. Introduction

Earthquakes are fast-slip processes of a fault, releasing stresses accumulated during the interseismic period. In the past few decades, advances in geodetic and seismic instrumentation have led to discoveries of much slower stress releasing modes, including slow slip events and accompanied seismic tremor as well as low frequency or very low frequency earthquakes (Dragert et al., 2001; Ito et al., 2007; Obara, 2002; Shelly et al., 2007). These various types of slow earthquakes mostly occur along the frictionally unstable to stable transition zone (e.g., Nishikawa et al., 2023; Obara, 2002; Shelly, 2017). Slow slip sometimes precedes large earthquakes (e.g., Kato et al., 2012; Meng et al., 2015; Socquet et al., 2017); understanding the role of slow slip in earthquake initiation is thus vital for earthquake hazard assessment and short-term forecasting (Obara & Kato, 2016).

In laboratory experiments, theoretical or numerical studies, earthquakes do not start abruptly. They are commonly preceded by extended nucleation phases dominated by slow slip (e.g., Kaneko et al., 2016; Latour et al., 2013; McLaskey & Lockner, 2014; Ohnaka & Shen, 1999; Passelègue et al., 2017; Rubin & Ampuero, 2005). On homogeneous faults, slow slip keeps accelerating and expanding within the nucleation zone until a critical nucleation length is reached, and then dynamic earthquake rupture propagation begins (e.g., Ohnaka & Shen, 1999; Rubin & Ampuero, 2005). Nucleation on heterogeneous faults is much more complex, as slow slip

and foreshocks can interact in a positive-feedback manner, resulting in episodic accelerations of slow slip and foreshocks leading up to the mainshock (Cattania & Segall, 2021; McLaskey, 2019).

In nature, however, it is challenging to observe slow slip related to earthquake nucleation (Abercrombie et al., 1995; Kaneko et al., 2017); such slip tends to generate only weak deformation signals at Earth's surface. For most earthquakes, no preseismic slip transients are detected or reported. However, in some cases, geodetic instruments capture slow slip signals in a large space-time window before large earthquakes. Prior to the 2011 M 9.0 Tohoku, Japan and 2014 M 8.2 Iquique, Chile megathrust earthquakes, for example, slow slip occurred over days to years before the mainshock and over tens of kilometers surrounding the mainshock rupture area (Ito et al., 2013; Socquet et al., 2017). This large-scale slow slip can be interpreted as an extensive nucleation of rupture, though it is still under debate whether slow slip occurs immediately before the mainshock (Bletery & Nocquet, 2023; Hirose et al., 2024). In some other cases, slow slip occurs but appears to be a trigger for nucleation, not the nucleation process itself. For instance, the 2014 Guerrero, Mexico slow slip event appeared to perturb stresses in a nearby region and promote the initiation of a M 7.3 earthquake (e.g., Radiguet et al., 2016).

Since slow slip is hard to observe directly, research often focuses on foreshocks: collections of small earthquakes that precede the mainshock. Foreshocks can be driven by slow slip (Kato et al., 2012; Meng et al., 2015) but can also trigger each other without the aid of slow slip (Ellsworth & Bulut, 2018; Felzer et al., 2015). Numerous efforts have been made to identify foreshock features that are likely indicative of slow slip, such as migrating, repeating, or accelerating foreshocks (Bouchon et al., 2011, 2013; Kato et al., 2012; Tape et al., 2018). However, there are still relatively few of these observations, and they often have significant uncertainty, so the role of slow slip in foreshock sequences remains controversial (Martínez-Garzón & Poli, 2024; Mignan, 2014; Peng & Lei, 2024). For example, before the 1999 Izmit M 7.6 strike-slip earthquake, there was a 44-min-long foreshock sequence, which may or may not be driven by slow slip (Bouchon et al., 2011; Ellsworth & Bulut, 2018). Sets of clustered foreshocks were also observed on the Minto Flats strike-slip fault zone, Alaska, where 20-s-long concurrent low- and high-frequency seismic signals are found before two $M \sim 3.7$ earthquakes, which again may represent foreshocks triggered by expanding slow slip (Tape et al., 2018). To fully understand clustered foreshocks, we need more examples to examine. However, it remains uncertain how common these foreshock sequences are on natural faults. They are challenging to detect; the foreshocks tend to create weak and overlapping seismic signals, hampering the identification and extraction of source properties.

The San Jacinto fault zone (SJFZ) is the most seismically active area in southern California, located to the south of the San Andreas Fault Zone (Figure 1). It consists of several right-lateral strike-slip fault branches. In the middle part of the SJFZ, the Anza seismic gap is devoid of recent large earthquakes; it has not ruptured in $M > 7$ earthquakes in the past 200 years, drawing much attention to its seismic risk. The abundant seismicity, complex slow and fast slip modes at depth (Inbal et al., 2017; Ross et al., 2017; Shaddox et al., 2021; Shearer et al., 2023; Wdowinski, 2009) and dense local seismic networks make the SJFZ an ideal site to study foreshocks during earthquake nucleation.

Here, we conduct a retrospective detection and source analysis of prolonged foreshock sequences along the SJFZ. We propose a new procedure to systematically detect clustered foreshock signals and extract the underlying moment-rate-power evolution. Our systematic analysis reveals that 19 out of 681 earthquakes have clustered foreshock sequences, which exhibit diverse patterns of source power build-up over the seconds before the mainshock. Our results shed new light into the complex earthquake nucleation along the base of the seismogenic zone.

2. Data and Methods

2.1. Synthetic Tests: Recovering Small Foreshocks' Moment-Rate Power Based on Phase Coherence

Our goal is to identify and understand foreshock sequences that occur over seconds in the lead-up to the mainshock. The seismograms in Figure 2, for example, are likely created by tens of foreshocks occurring over around 10 s. Such closely spaced foreshocks can be difficult to identify and disentangle because their waveforms overlap. So we have developed a modified phase coherence approach (also known as matched field) to detect these small event clusters and determine their source power.

Following previous work (Barajas et al., 2024; Corciulo et al., 2012; Gibbons & Ringdal, 2006; Hawthorne & Ampuero, 2018; Wang et al., 2015), we use an empirical Green's function approach to remove the seismic wave's

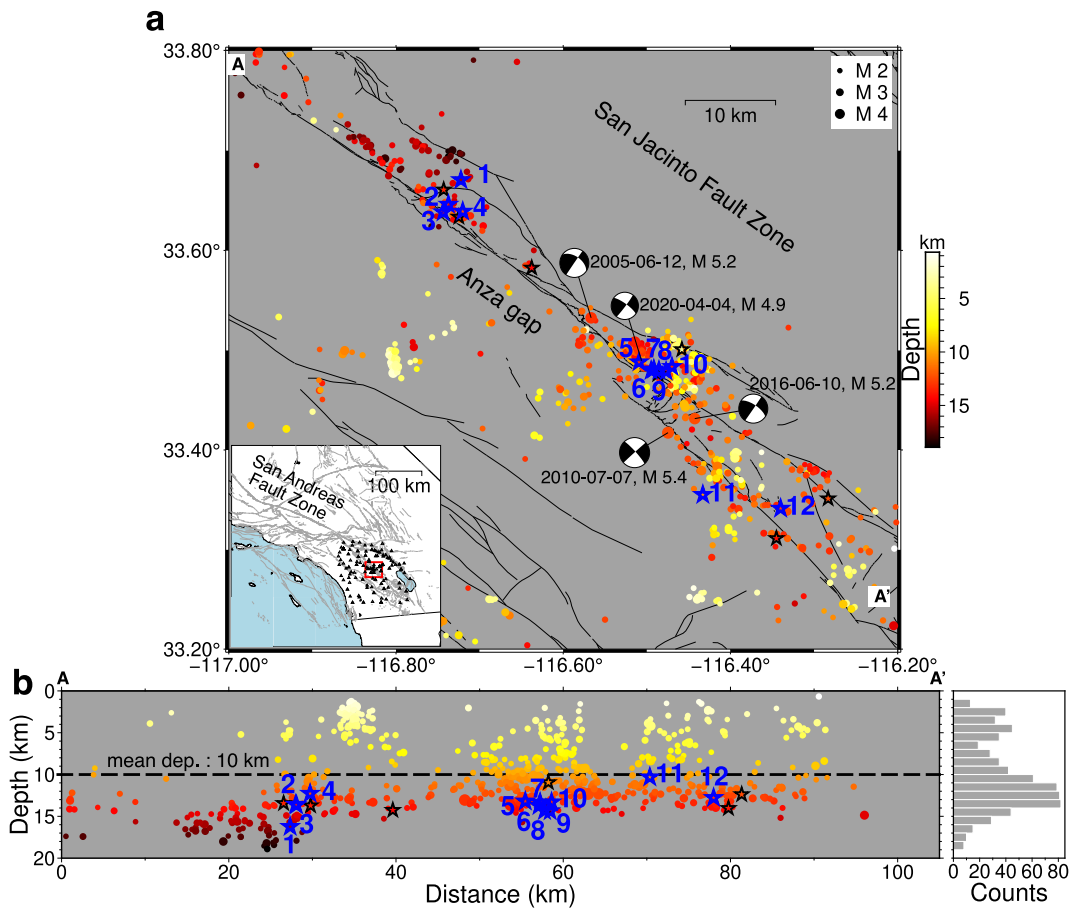

Figure 1. Location map of seismicity and clustered foreshock sequences along the San Jacinto fault zone. (a) The colored dots are 699 $M \geq 2.5$ seismicity within 2000–2023, obtained from the Southern California Seismic Network. Focal mechanisms are shown for $M > 4.5$ events. The black lines show active faults, while the inset map shows the tectonic background of the study area with black triangles denoting seismic stations used (network codes: CI, AZ, PB, PY, II, and NP). (b) The depth cross section along profile AA′ shown in (a). Stars in (a and b) denote the 19 events with clustered foreshock sequences. The blue outlined stars are 12 events shown in Figures 2 and 4. The dashed line denotes the mean depth of all events. The right panel in (b) shows the histogram of earthquake depth.

path effect by cross-correlating the mainshock signal with a proposed foreshock signal at a number of stations. This isolates the phase differences of any foreshock sequence's moment rate function (MRF). We compute cross spectra ($\hat{x}_k$) between the mainshock record ($d_{m,k}$) and foreshock record ($d_{f,k}$) in the frequency domain,

$$\hat{x}_k = \hat{d}^*_{m,k}\, \hat{d}_{f,k} \tag{1}$$

where k is station index and * denotes complex conjugate. The phase differences of target foreshock MRF with respect to template mainshock MRF should be the same at all stations, so we can detect unknown target sequences by further looking for phase similarities of $\hat{x}_k$ among stations, even if the target sequence has a more complex or longer MRF than the template event. For detection purposes, Hawthorne and Ampuero (2018) have computed a coherence parameter C_p at a pair of stations 1 and 2,

$$C_p = \mathrm{Re}\left(\frac{\hat{x}_1^* \hat{x}_2}{|\hat{x}_1||\hat{x}_2|}\right) \tag{2}$$

More explicit details and real-world uses are given by Hawthorne and Ampuero (2018). This method is ideal for our use. We will be able to detect collections of foreshocks that have paths similar to the mainshock even though the more complex foreshock MRFs will downgrade the similarity between foreshock and mainshock waveforms.

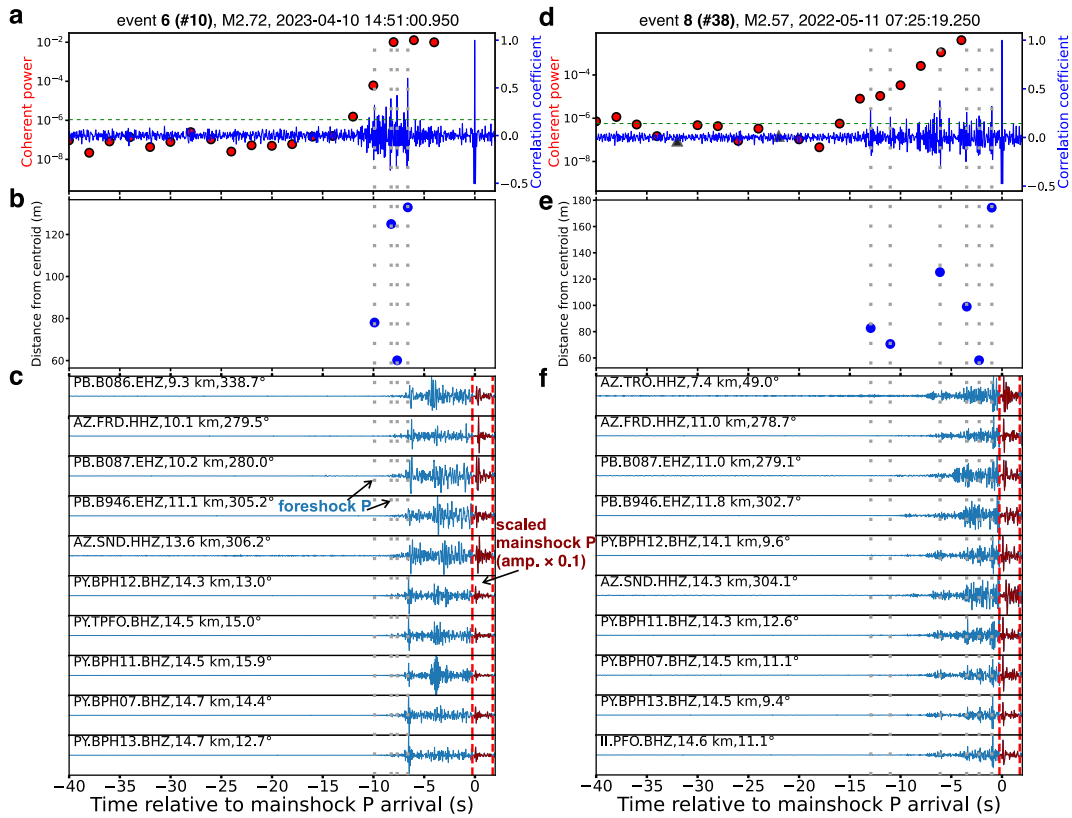

Figure 2. Examples of identified clustered foreshock sequences along the San Jacinto fault zone. (a–c) Panel (c) shows the vertical seismic waveforms at 10 closest stations for event 6 (Figure 1), filtered between 2 and 8 Hz. Note that for clarity of foreshock signals, the mainshock P wave template window between two red dashed lines is scaled down by 10 relative to the rest of the signal. (a) The corresponding coherent power (in logarithmic scale) calculated from the modified phase-coherence method, with red circles and gray triangles being positive and negative values, respectively. The coherent power series stops at −4 s to avoid smearing from the mainshock. The blue line denotes the average cross-correlation coefficients obtained from matched-filter analysis, with the green dashed lines showing 9 times the median absolute deviation of the cross-correlation trace between −200 and −50 s. The gray vertical dotted lines mark the P arrival times of individual foreshocks. (b) Blue dots show the distance of foreshocks from mainshock centroid (Text S1 in Supporting Information S1). (d–f) Similar to (a–c) but for event 8.

In this work, we take a step beyond detection. We modify the normalization term (denominator) of the phase coherence calculation in Equation 2 to be the product of template power at two stations (see also Hawthorne et al., 2019). Specifically, we compute,

$$E_c = \mathrm{Re}\left(\frac{\hat{x}_1^* \hat{x}_2}{\left|\hat{d}_{m,1}\right|^2 \left|\hat{d}_{m,2}\right|^2}\right) \tag{3}$$

E_c is termed coherent power, which provides an unbiased (if sometimes noisy) estimate of $\sum {M'_{0\_\mathrm{target}}}^2 / \sum {M'_{0\_\mathrm{temp}}}^2$, where M'_{0_target} and M'_{0_temp} are the MRF of the target and template event, respectively (see Text S1 in Supporting Information S1 for more details on derivation).

We conduct extensive synthetic tests to demonstrate the robustness of the new procedure. We generate synthetic seismic records composed of three-component waveforms at 10 stations for plausible template mainshocks and target foreshock sequences (Figure 3a). This is done by convolving template and target MRFs with the same set of random Green's functions (white noises tapered by exponential decay). The target event waveforms are aligned with the template waveforms and are embedded within longer windows of random noise (Figure 3a).

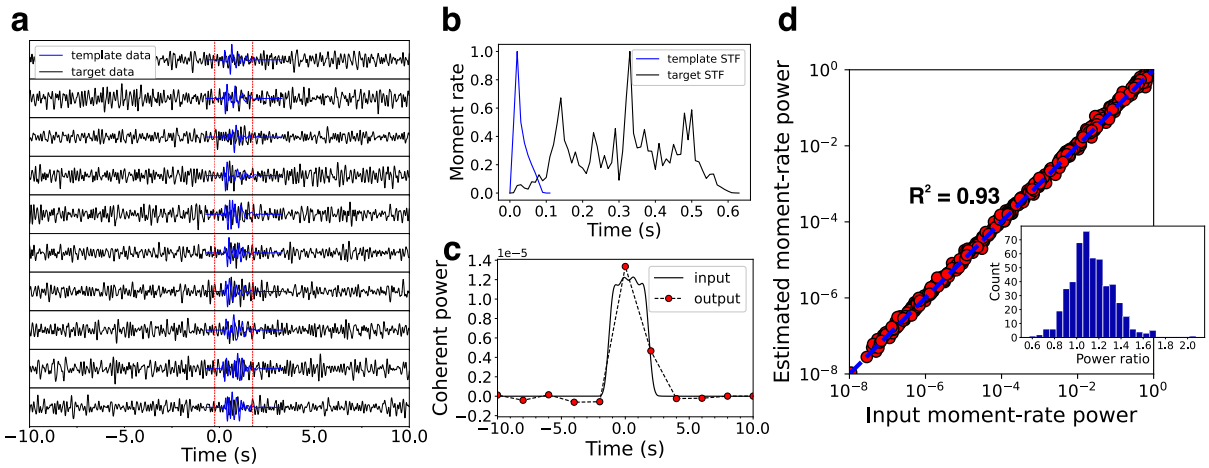

Figure 3. Synthetic tests of the phase coherence method to recover the moment-rate power of foreshock sequences. (a) A test sample of synthetic template (blue) and target waveforms (black). Target event waveforms are aligned with template event waveforms and embedded in a longer window with random noise added. Both waveforms are bandpass filtered within 2–8 Hz. (b) Input MRFs (normalized) for the template event (blue) and randomly generated small target event (black). To mimic a foreshock sequence, the moment rate function (MRF) of the target event is designed to be much longer and complex than that of the template event. (c) Comparison of input coherent-power series from target-event MRF (solid line) and output coherent power series (within 2–8 Hz, dashed dotted line) calculated by phase coherence, with a step of 2 s. The input coherent-power series is calculated by summing the square of tapered target-event MRF (within 2–8 Hz) in 4-s long moving windows, normalized by the total template-event MRF power. (d) Consistency of the input and estimated moment-rate power from 500 realizations, by comparing the value of two power series at time zero (c). The blue dashed line shows a 1:1 line. The inset histogram shows the distribution of the ratio between estimated and input power.

The target MRF is designed to mimic a foreshock sequence; it is randomly generated and designed to be small in amplitude but longer and more complex than the template event MRF. In a sample test shown in Figure 3b, the template MRF is ∼0.1-s long while the target MRF is ∼0.6-s long with multiple peaks. Once we have the synthetic seismograms, we compute a coherent power time series. At each station and component, we cross-correlate the template seismogram (2 s long) with the target seismogram. Then we consider a range of overlapping 4-s windows from cross-correlation traces with a step of 2 s. For each window, we calculate the power in the 2–8 Hz band that is coherent among stations. The power is averaged over all station pairs and over all components. This is our estimate of $\sum M'_{0\_\text{target}}{}^2 / \sum M'_{0\_\text{temp}}{}^2$, as described above.

If we examine power at the beginning and end of our synthetic seismograms, where data are dominated by incoherent noise, the calculated coherent power is scattered around zero (Figure 3c), as expected. Note that the coherent power can be negative, particularly in noise windows. The coherent power is, after all, only an estimate of the moment rate power; it is the real part of some normalized cross spectra of the data, averaged over frequency (see Equation 3). However, the coherent power becomes clearly positive and significantly larger than the background scatter for about 4 s in the middle of the seismogram. This is when the analysis window includes at least part of the 0.6-s-long target MRF. The coherent power amplitudes are also as expected given the power we input into synthetic MRFs (Figure 3c).

We further perform 500 random tests by re-generating target event MRFs and Green's functions, followed by synthetic waveform convolution, noise addition, and coherent-power calculation. For each test sample, we compare the power at time zero of the average coherent-power series with that of the input power series (e.g., Figure 3c). The method robustly recovers the 2-8-Hz moment-rate power of the target event over a wide range of inputs (10^{-8} to 1) with a 1-sigma accuracy around 20% and a R^2 (coefficient of determination) score of 0.93 (Figure 3d). The consistency indicates that this modified phase-coherence method works well to detect target events with more complex sources than the template event. It also retrieves their relative moment-rate power with a precision around 20%; this will be more than precise enough for our foreshock analysis. We note, however, that the method relies on having known templates with similar focal mechanisms at nearby locations. That reliance could hamper the method's use for real-time monitoring or further extractions of additional source parameters.

2.2. Identification of Clustered Foreshock Sequences Along the SJFZ

We use the phase-coherence power calculation to search for clustered foreshocks in the seconds before all 699 $M \geq 2.5$ earthquakes that occurred from 2000 to 2023 along the SJFZ. In our analysis, we first extract high-quality multi-station, multi-channel P-wave template waveforms by selecting 2-s long windows around the mainshock P-wave arrivals and requiring them to have a high signal-to-noise ratio (>5). As a result, 681 events are retained, with the majority recorded by over 15 stations within 50 km epicentral distance (Figure S1 in Supporting Information S1). As for the synthetics tests, we cross-correlate the template waveforms with the pre-mainshock seismograms and then compute the power that is coherent across stations in 4-s windows, starting every 2 s in the 200 s before the mainshock. Our goal is to identify clustered foreshock sequences. So we first identify events which have a median coherent power within the last 6–50 s that exceeds 10 times the absolute background coherent power. Then we use a standard matched filter approach to check that the power comes from multiple foreshocks. We cross correlate the mainshock template with the pre-mainshock seismogram and retain only events that have at least two peaks in the last 20 s. This additional criteria helps identify foreshocks with clustered features instead of only a single foreshock (see Text S1 in Supporting Information S1 for more details on detection threshold and data processing).

3. Results

We find that 19 (M 2.5–4.7, Table S1 and Figures S2, S3 in Supporting Information S1) among 681 events have clustered foreshocks. The 19 events are only a small fraction of the total analyzed events; a collection of all 681 coherent-power series shows that most events are not preceded by elevated coherent power (Figure S4 in Supporting Information S1). However, the newly detected clustered foreshocks are still significant, as such accelerating immediate foreshocks have rarely been observed in nature (e.g., Peng & Lei, 2024; Tape et al., 2018). The detections of 19 sequences remain significant when we vary the parameters of frequency band or window length during coherent-power calculation (Figures S5 and S6 in Supporting Information S1).

Note that our 19 detections exclude a number of earthquakes that appear to have a single immediate foreshock. For example, 12 earthquakes, including the 2016 M 5.2 Borrego Springs event, appear to have a foreshock within 4 s of the mainshock. These events show elevated coherent power in the last time window and only one cross-correlation peak (Figure S7 in Supporting Information S1). Our focus, though, is on the evolution of clustered foreshock sequences, so we exclude such events for further discussions.

The identified sequences are mostly located along the central fault strand of the SJFZ (Figure 1a). All 19 sequences identified via coherent power are also clearly visible as 5 to 20-s-long seismic signals that lead up to the mainshock (Figures 2a and 2b; Figure S3 in Supporting Information S1). For instance, Figure 2 shows the sequences before event 6 and 8, with the enlarged pre-P waveforms showing enduring seismic signals in the 2–8 Hz band. The coherent power series provides new constraints on the temporal evolution of total source power around the template, which is not available from the matched-filter cross-correlation coefficients. During the time periods of moment-rate power build-up, the average correlations exhibit multiple peaks with high significance, validating that multiple sources radiate P waves intensely within seconds. A search over 3-D location grids shows that these significant correlation peaks correspond to at least 4 or 6 foreshocks located within ∼130 m from their respective mainshock centroids (Text S1 and Figures S8–S12 in Supporting Information S1). The foreshock location appears to change with time; we see a changing distance from the mainshock centroid in Figures 2b and 2e. However, the ∼130-m spatial distribution of foreshocks is small enough that foreshocks could be migrating within the rupture zone of the $M \sim 2.5$ mainshocks; a M 2.5 earthquake with a 0.3 to 30-MPa stress drop has a diameter around 60–270 m.

Figure 4 shows the precursory coherent-power evolution for 12 selected sequences (see Figure 1 for location). Results for the remaining 7 events are provided in Figure S3 in Supporting Information S1. Foreshock sequences generally show a growth in power during the tens of seconds before the mainshock, but there is variability in the duration and smoothness of the build-up phase. For example, for event 8, the build-up phase lasts ∼13 s, while event 9 has a ∼5 s-long build-up phase. The smoothness of the build-up phase also varies: events 1, 2, 5, 6, 8, 9, 10, and 12 are preceded by relatively continuous power build-up; power build-up is more episodic before events 3, 4, 7, and 11, and before the remaining 7 events shown in Figure S3 in Supporting Information S1. Note that power build-up can only be resolved for time periods longer than 4 s, as the windowing smooths over that interval.

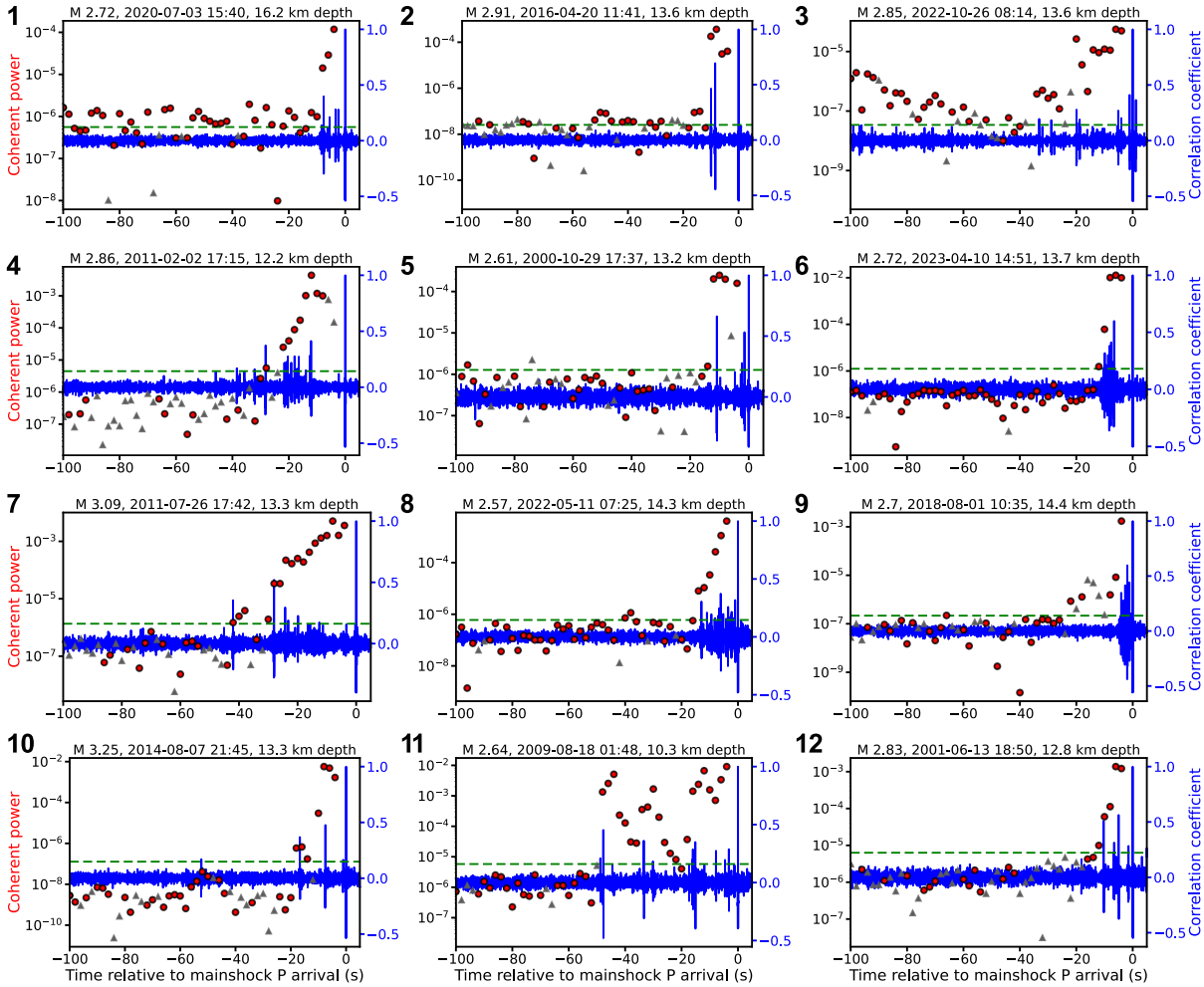

Figure 4. Elevated coherent power before 12 identified earthquakes along the San Jacinto fault zone. Red circles and gray triangles denote positive and negative coherent power, respectively, while blue lines are average cross-correlation coefficients (see Main Text). Green dashed lines denote 9 times the median absolute deviation of the cross-correlation trace between −200 and −50 s. Results for the remaining 7 events are shown in Figure S3 in Supporting Information S1. The mainshock information is shown in the title. The event labels are marked alongside with locations shown in Figure 1.

Interestingly, all 19 identified clustered foreshock sequences occur near the bottom of the seismogenic zone of the SJFZ (Figure 1b). The depths of the identified sequences range from 10.3 to 16.2 km (mean: ∼13.4 km), all below the mean depth of the whole catalog (∼10.0 km). The proportion of events having clustered foreshocks within the 10.3–16.2 km depth range is ∼5.3%, higher than the overall rate of clustered foreshocks (∼2.8%). This indicates a tendency of clustered foreshocks to occur at the deeper part of the seismogenic zone.

4. Discussion

Through a systematic search before 681 $M \geq 2.5$ seismicity along the SJFZ, we find 19 clustered foreshock sequences, where source power is elevated in the 5–20 s before the mainshock. These rare observations are useful, as they may be associated with nucleation processes before M 2.5–4.7 natural earthquakes. Two features of our detections are of particular interest: the build-up of source power before mainshocks and the tendency for clustered foreshock sequences to occur near the base of the seismogenic zone. This may suggest that foreshocks cluster and build up in power under some range of fault conditions.

The moment-rate power build-up toward the mainshocks indicates that the observed foreshocks tend to grow in magnitude or frequency toward the mainshock time. This behavior differs from typical mainshock-aftershock sequences (Mogi, 1963), where earthquakes are followed by smaller aftershocks and the seismicity rate decays with time (Omori, 1894). At least three possible scenarios could account for the moment-rate power growth. In the

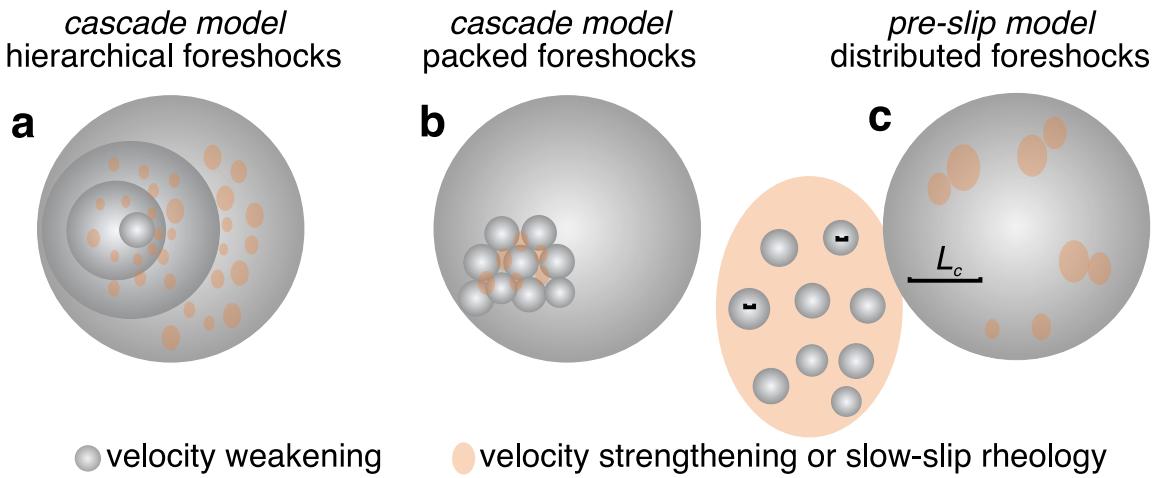

Figure 5. Sketch of possible fault ingredients for extended source-power build-up during foreshocks. (a) Different-sized asperities nested in a hierarchical structure. Gray indicates velocity-weakening, unstable patches capable of generating earthquakes, while orange indicates velocity-strengthening, stable patches or patches with slow-slip rheology. (b) Densely packed similar-sized foreshocks and a nearby larger mainshock. (c) Sparsely distributed foreshocks embedded within velocity-strengthening or slow-slip zones, with the mainshock patch having larger average L_c than foreshocks.

first scenario, there are hierarchical asperities on the fault (Ellsworth & Beroza, 1995; Ide & Aochi, 2005; Okuda & Ide, 2018), resulting in sequential ruptures from smaller asperities to larger ones (Figure 5a). In the second scenario, there are numerous densely packed, similarly sized small asperities that break more and more often with time (Figure 5b). These two scenarios are types of cascade triggering (Ellsworth & Bulut, 2018), where foreshocks trigger each other via event-to-event static or dynamic stress transfer.

The third scenario, on the other hand, is a preslip model, where foreshocks are mainly driven by slow slip (Bouchon et al., 2011; Kato et al., 2012; Meng et al., 2015; Tape et al., 2018). In this scenario, foreshock asperities are more sparsely distributed; they rupture increasingly frequently in response to accelerating slow slip in the nucleation area (Figure 5c). All three scenarios can explain the sequential rupture of asperities building up in power. But for the cascade-triggering scenarios 1 and 2 to explain the seconds-long power build-up, which is much longer than the duration of individual foreshocks, some physical process for delayed triggering needs to be invoked; this could be an external process like slow slip or fluid flow (e.g., Hill et al., 1993; Kaneko et al., 2019), or it could be a minimum timescale for foreshock nucleation (as in, e.g., Gomberg et al., 2005).

Further insights about the physical processes involved in nucleation may come from the location of clustered foreshock sequences. In the shallow seismogenic zone of a fault, the friction generally decreases when slip velocity increases (it is velocity-weakening, VW), while as the fault goes deeper, conditions transition to a regime where the friction increases when sliding velocity increases (velocity-strengthening, VS). The VW and VS regimes promote unstable and stable fault slip, respectively (Scholz, 1998). The clustered foreshocks identified along the base of the seismogenic zone of the SJFZ are likely located near the transition from VW to VS friction. Complexity in this region could facilitate complex fault slip patterns (Ando et al., 2010; Barnes et al., 2020; Dublanchet et al., 2013; Luo & Ampuero, 2018; Skarbek et al., 2012). This transition zone of the SJFZ has been widely studied by various approaches. For instance, Wdowinski (2009) used geodetic and seismic data to identify deep creep (10–17 km depth) that could promote excess small earthquakes near the base of the seismogenic zone. Abolfathian et al. (2019) used high-resolution stress inversions to show the change of stress field at >9 km depth, implying a change of fault mechanical behavior at the transition zone. Numerical simulations have shown that frictional heterogeneity in the transition zone can permit observed shallow geodetic fault locking (Jiang & Fialko, 2016). Previous studies have also observed slow-slip transients near this zone of the SJFZ using geodetic data and repeating earthquakes (Inbal et al., 2017; Shaddox et al., 2021). The inferred repeating earthquakes and aseismic-slip transients overlap spatially with the clustered foreshock sequences in this study (Figure S13 in Supporting Information S1).

Our identified foreshock sequences differ from another phenomenon identified near the seismic-aseismic transition: from tectonic tremor. The identified foreshocks have similar impulsive P waves (e.g., Figure 2) as the

mainshock and thus likely reflect fast-slip seismic ruptures of smaller asperities. This implies that their source processes are different from other slower seismic processes such as tectonic tremor widely found along the base of the seismogenic zone near Parkfield (Shelly, 2017) in the central San Andreas fault. The clustered foreshock sequences may bear more source similarities to repeating or hierarchical earthquakes (Okuda & Ide, 2018; Uchida et al., 2012): they both interact with nearby aseismically slipping regions. Compared to repeaters re-rupturing the same asperity, clustered foreshock sequences may involve more frequent ruptures of different small asperities. Globally, larger-scale days-to-months long slow slip events are also observed near the VW to VS transition in subduction zones (e.g., Dragert et al., 2001; Ito et al., 2007; Nishikawa et al., 2023; Obara & Kato, 2016). Though frictional transition appears to be common fault conditions, the physical mechanism that creates extensive and various-scale slow slip remains unclear (Harbord et al., 2017; Huang & Hawthorne, 2022; Ide & Beroza, 2023; Liu & Rice, 2005; Rubin, 2008).

Our observations of closely spaced foreshocks and mainshocks could imply that the transition zone on the SJFZ contains numerous patches with a range of sizes and frictional properties. Foreshock sequences may occur in the transition zone because rupture starts rapidly on a small unstable patch, slows when it reaches a stable region at the patch edge, but then continues and accelerates into another, larger foreshock when it reaches a nearby patch. These foreshocks may cascade into a mainshock. Alternatively, our observations could imply that the frictional properties of the transition zone promote preslip. The frictional properties of the fault control the earthquake nucleation size L_c: the smallest area that can accelerate independent of its surroundings (Chen & Lapusta, 2019; Harbord et al., 2017). The total mainshock area may have a relatively large L_c, as expected near the VW to VS transition. This large L_c would allow a large (~100-m) region to accelerate aseismically. But small foreshock patches within that region could have smaller L_c and permit localized seismic slip during the mainshock nucleation. It is noteworthy that cascade and pre-slip scenarios may oversimplify nucleation processes (Martínez-Garzón & Poli, 2024). The combined effects of cascade and preslip are also possible, as recent laboratory studies show that a fault patch may have temporally shrinking L_c caused by increasing loading rate and is finally ignited by a small foreshock (Guérin-Marthe et al., 2019; McLaskey, 2019). During this process, slow slip and foreshocks can interact in a positive-feedback manner, resulting in overall slow acceleration of foreshocks (Cattania & Segall, 2021).

With just our observations, it is not possible to distinguish the above three scenarios, especially based on seismological data alone. Cascade and pre-slip scenarios could result in similar characteristics in foreshock sequences, such as clustered or accelerating foreshocks (e.g., Bouchon et al., 2011; Ellsworth & Bulut, 2018). Pre-slip models involve slow-slip propagation thus may result in systematic migrations of foreshocks. Our observations show that four to six individual foreshocks before two events are evolving in space (Figure 2) but the pattern is not systematic. Geodetic data are critical to nail down the relative contribution of aseismic and seismic deformation (e.g., Socquet et al., 2017), but is difficult to be applied to seconds-long scale here. Nevertheless, some speculations might be made to compare our results with existing laboratory or natural earthquake observations. For example, if we go ahead and speculate that foreshocks are embedded in a pre-slip region (scenario 3), we can use our observations to make some inferences about the evolution of slip during nucleation. To do so, we assume that foreshocks are simply caused by aseismic loading, such that the foreshock rate is proportional to the slow-slip moment rate. If we assume that foreshock magnitudes are independent of time, this means that the moment-rate-power growth rate we observe should be proportional to the slow-slip moment rate. We find that for three mainshocks (event 6, 8, and 12) which have simple power build-up phases, the moment-rate power evolution can be well fit by an exponential or power-law function (Figure S11 in Supporting Information S1). Such evolutionary functions are consistent with exponential accelerations of rupture velocity or seismicity rate seen in $M < 0$ laboratory earthquake experiments (Hulbert et al., 2020; Latour et al., 2013; Passelègue et al., 2017; Yoshida & Ogawa, 2004), stacked foreshock rates of $M > 7$ interplate earthquakes (Bouchon et al., 2013), and pre-mainshock ($M > 7$) stacked GPS time series (Bletery & Nocquet, 2023). This consistency could imply that nucleation phases obey similar functions across different scales, but the scaling is uncertain and warrants further investigation.

Our observations also have implications for detectability of natural earthquake nucleations. Numerical simulations and laboratory experiments show that fault conditions such as stress heterogeneity (Cattania & Segall, 2021; McLaskey, 2019), geometry (Yamashita et al., 2021) or pore fluid pressure (Goebel et al., 2024) control the scale of earthquake nucleation. We show that only a small subset (19 out of 681) of earthquakes near the base of the seismogenic zone of the SJFZ have detectable nucleation signals. Although our observations of clustered

foreshocks may be partially limited by resolution and further detections are possible, our results may indicate that nucleation scales depend on fault conditions and vary along the same fault zone. Under the framework of frictional heterogeneity, the majority of analyzed events (662) that do not show detectable extended nucleation may occur on fault patches with less VW/VS heterogeneity and/or less density than that outlined in Figure 5. As more observations accrue, it would be interesting to further test this hypothesis as well as explore other types of heterogeneity such as stress, geometry or fluids in controlling the nucleation scale of natural earthquakes. On the other hand, it is unclear whether nucleation scales depend on mainshock magnitudes. However, the measurement of nucleation time scales for natural earthquakes is somewhat ambiguous because the nucleation process may consist of several stages (e.g., Martínez-Garzón & Poli, 2024; Socquet et al., 2017). The 5 to 20-s-long seismic signals prior to 8 events (M 2.57–3.25) with relatively continuous source power growth in our study (e.g., Figures 2a and 2d) could result from the last stage of nucleation, which appears to be shorter than the duration of similar clustered seismic signals preceding two $M \sim 3.7$ events (22 and 24 s) in Alaska (Figure S12 in Supporting Information S1, Tape et al., 2018). The shorter nucleation preceding these smaller events are enticing, and warrants further work to assess whether temporal and spatial nucleation scales correlate with mainshock magnitude. To address this problem, we envision a systematic analysis across different magnitude ranges and tectonic settings.

Conflict of Interest

The authors declare no conflicts of interest relevant to this study.

Availability Statement

Waveform data were downloaded from the Incorporated Research Institutions for Seismology Data Management Center, and the Southern California Earthquake Data Center, including data mainly from seismic networks CI (California Institute of Technology and United States Geological Survey Pasadena, 1926), AZ (Frank, 1982), PB (Plate Boundary Observatory Borehole Seismic Network, https://www.fdsn.org/networks/detail/PB/), PY (Frank, 2014), II (EarthScope Consortium, 1986), NP (U.S. Geological Survey, 1931). The earthquake catalog in the SJFZ was available at the ANSS Comprehensive Earthquake Catalog (https://earthquake.usgs.gov/earthquakes/search/). The catalog of identified earthquakes with clustered foreshock sequences is available in the Table S1 in Supporting Information S1. Seismic data and preprocessing are based on the open software Obspy (https://docs.obspy.org/). Example code and data for coherent power calculation can be found at Huang and Hawthorne (2025).

Acknowledgments
This study is supported by the National Natural Science Foundation of China (Grant 42474076) and the Fundamental Research Funds for the Central Universities. The methodological development was particularly supported by the UK's Natural Environment Research Council Grant NE/S00968X/1. The authors are grateful to Jean-Paul Ampuero for physical and methodological discussions; this work was motivated in part by an unpublished search for tremor-like precursors by J.C.H. and J.-P. Ampuero in 2013–2014. We thank Editor Dr. Germán Prieto, Associate Editor Dr. Patricia Martínez-Garzón and two anonymous reviewers for their constructive reviews, which greatly improved this paper.

References

Abercrombie, R. E., Agnew, D. C., & Wyatt, F. K. (1995). Testing a model of earthquake nucleation. *Bulletin of the Seismological Society of America*, *85*(6), 1873–1878. https://doi.org/10.1785/bssa0850061873

Abolfathian, N., Martínez-Garzón, P., & Ben-Zion, Y. (2019). Spatiotemporal variations of stress and strain parameters in the San Jacinto fault zone. *Pure and Applied Geophysics*, *176*(3), 1145–1168. https://doi.org/10.1007/s00024-018-2055-y

Ando, R., Nakata, R., & Hori, T. (2010). A slip pulse model with fault heterogeneity for low-frequency earthquakes and tremor along plate interfaces. *Geophysical Research Letters*, *37*(10). https://doi.org/10.1029/2010gl043056

Barajas, A., Shapiro, N. M., & Prieto, G. (2024). Differential phase analysis for volcanic tremor detection and source location. *Journal of Geophysical Research: Solid Earth*, *129*(10), e2024JB029010. https://doi.org/10.1029/2024jb029010

Barnes, P. M., Wallace, L. M., Saffer, D. M., Bell, R. E., Underwood, M. B., Fagereng, A., et al. (2020). Slow slip source characterized by lithological and geometric heterogeneity. *Science Advances*, *6*(13), eaay3314. https://doi.org/10.1126/sciadv.aay3314

Bletery, Q., & Nocquet, J. M. (2023). The precursory phase of large earthquakes. *Science*, *381*(6655), 297–301. https://doi.org/10.1126/science.adg2565

Bouchon, M., Karabulut, H., Aktar, M., Özalaybey, S., Schmittbuhl, J., & Bouin, M. P. (2011). Extended nucleation of the 1999 M w 7.6 Izmit earthquake. *Science*, *331*(6019), 877–880. https://doi.org/10.1126/science.1197341

Bouchon, M., Durand, V., Marsan, D., Karabulut, H., & Schmittbuhl, J. (2013). The long precursory phase of most large interplate earthquakes. *Nature Geoscience*, *6*(4), 299–302. https://doi.org/10.1038/ngeo1770

California Institute of Technology and United States Geological Survey Pasadena. (1926). Southern California seismic network [Dataset]. *International Federation of Digital Seismograph Networks*. https://doi.org/10.7914/SN/CI

Cattania, C., & Segall, P. (2021). Precursory slow slip and foreshocks on rough faults. *Journal of Geophysical Research: Solid Earth*, *126*(4), e2020JB020430. https://doi.org/10.1029/2020jb020430

Chen, T., & Lapusta, N. (2019). On behaviour and scaling of small repeating earthquakes in rate and state fault models. *Geophysical Journal International*, *218*(3), 2001–2018. https://doi.org/10.1093/gji/ggz270

Corciulo, M., Roux, P., Campillo, M., Dubucq, D., & Kuperman, W. A. (2012). Multiscale matched-field processing for noise-source localization in exploration geophysics. *Geophysics*, *77*(5), KS33–KS41. https://doi.org/10.1190/geo2011-0438.1

Dragert, H., Wang, K., & James, T. S. (2001). A silent slip event on the deeper Cascadia subduction interface. *Science*, *292*(5521), 1525–1528. https://doi.org/10.1126/science.1060152

Dublanchet, P., Bernard, P., & Favreau, P. (2013). Interactions and triggering in a 3-D rate-and-state asperity model. *Journal of Geophysical Research: Solid Earth*, *118*(5), 2225–2245. https://doi.org/10.1002/jgrb.50187

EarthScope Consortium. (1986). Global seismograph network - II [Dataset]. *International Federation of Digital Seismograph Networks*. https://doi.org/10.7914/SN/II

Ellsworth, W. L., & Beroza, G. C. (1995). Seismic evidence for an earthquake nucleation phase. *Science*, *268*(5212), 851–855. https://doi.org/10.1126/science.268.5212.851

Ellsworth, W. L., & Bulut, F. (2018). Nucleation of the 1999 Izmit earthquake by a triggered cascade of foreshocks. *Nature Geoscience*, *11*(7), 531–535. https://doi.org/10.1038/s41561-018-0145-1

Felzer, K. R., Page, M. T., & Michael, A. J. (2015). Artificial seismic acceleration. *Nature Geoscience*, *8*(2), 82–83. https://doi.org/10.1038/ngeo2358

Frank, V. (1982). ANZA regional network [Dataset]. *International Federation of Digital Seismograph Networks*. https://doi.org/10.7914/SN/AZ

Frank, V. (2014). Piñon flats observatory array [Dataset]. *International Federation of Digital Seismograph Networks*. https://doi.org/10.7914/SN/PY

Gibbons, S. J., & Ringdal, F. (2006). The detection of low magnitude seismic events using array-based waveform correlation. *Geophysical Journal International*, *165*(1), 149–166. https://doi.org/10.1111/j.1365-246x.2006.02865.x

Goebel, T. H., Schuster, V., Kwiatek, G., Pandey, K., & Dresen, G. (2024). A laboratory perspective on accelerating preparatory processes before earthquakes and implications for foreshock detectability. *Nature Communications*, *15*(1), 5588. https://doi.org/10.1038/s41467-024-49959-7

Gomberg, J., Reasenberg, P., Cocco, M., & Belardinelli, M. E. (2005). A frictional population model of seismicity rate change. *Journal of Geophysical Research*, *110*(B5). https://doi.org/10.1029/2004jb003404

Guérin-Marthe, S., Nielsen, S., Bird, R., Giani, S., & Di Toro, G. (2019). Earthquake nucleation size: Evidence of loading rate dependence in laboratory faults. *Journal of Geophysical Research: Solid Earth*, *124*(1), 689–708. https://doi.org/10.1029/2018jb016803

Harbord, C. W., Nielsen, S. B., De Paola, N., & Holdsworth, R. E. (2017). Earthquake nucleation on rough faults. *Geology*, *45*(10), 931–934. https://doi.org/10.1130/g39181.1

Hawthorne, J. C., & Ampuero, J. P. (2018). A phase coherence approach to identifying co-located earthquakes and tremor. *Geophysical Journal International*, *209*(2), 623–642.

Hawthorne, J. C., Thomas, A. M., & Ampuero, J. P. (2019). The rupture extent of low frequency earthquakes near Parkfield, CA. *Geophysical Journal International*, *216*(1), 621–639. https://doi.org/10.1093/gji/ggy429

Hill, D. P., Reasenberg, P. A., Michael, A., Arabaz, W. J., Beroza, G., Brumbaugh, D., et al. (1993). Seismicity remotely triggered by the magnitude 7.3 Landers, California, earthquake. *Science*, *260*(5114), 1617–1623. https://doi.org/10.1126/science.260.5114.1617

Hirose, H., Kato, A., & Kimura, T. (2024). Did short-term preseismic crustal deformation precede the 2011 great Tohoku-oki earthquake? An examination of stacked tilt records. *Geophysical Research Letters*, *51*(12), e2024GL109384. https://doi.org/10.1029/2024gl109384

Huang, H., & Hawthorne, J. (2025). Oldyellow9451/Coherent-energy-calculation-by-phase-coherence: Earthquake detection and power estimation based on phase coherence (foreshock_analysis) [Software]. *Zenodo*. https://doi.org/10.5281/zenodo.17518645

Huang, H., & Hawthorne, J. C. (2022). Linking the scaling of tremor and slow slip near Parkfield, CA. *Nature Communications*, *13*(1), 5826. https://doi.org/10.1038/s41467-022-33158-3

Hulbert, C., Rouet-Leduc, B., Jolivet, R., & Johnson, P. A. (2020). An exponential build-up in seismic energy suggests a months-long nucleation of slow slip in Cascadia. *Nature Communications*, *11*(1), 4139. https://doi.org/10.1038/s41467-020-17754-9

Ide, S., & Aochi, H. (2005). Earthquakes as multiscale dynamic ruptures with heterogeneous fracture surface energy. *Journal of Geophysical Research*, *110*(B11). https://doi.org/10.1029/2004jb003591

Ide, S., & Beroza, G. C. (2023). Slow earthquake scaling reconsidered as a boundary between distinct modes of rupture propagation. *Proceedings of the National Academy of Sciences*, *120*(32), e2222102120. https://doi.org/10.1073/pnas.2222102120

Inbal, A., Ampuero, J. P., & Avouac, J. P. (2017). Locally and remotely triggered aseismic slip on the central San Jacinto Fault near Anza, CA, from joint inversion of seismicity and strainmeter data. *Journal of Geophysical Research: Solid Earth*, *122*(4), 3033–3061. https://doi.org/10.1002/2016jb013499

Ito, Y., Hino, R., Kido, M., Fujimoto, H., Osada, Y., Inazu, D., et al. (2013). Episodic slow slip events in the Japan subduction zone before the 2011 Tohoku-Oki earthquake. *Tectonophysics*, *600*, 14–26. https://doi.org/10.1016/j.tecto.2012.08.022

Ito, Y., Obara, K., Shiomi, K., Sekine, S., & Hirose, H. (2007). Slow earthquakes coincident with episodic tremors and slow slip events. *Science*, *315*(5811), 503–506. https://doi.org/10.1126/science.1134454

Jiang, J., & Fialko, Y. (2016). Reconciling seismicity and geodetic locking depths on the Anza section of the San Jacinto fault. *Geophysical Research Letters*, *43*(20), 10–663. https://doi.org/10.1002/2016gl071113

Kaneko, Y., Carpenter, B. M., & Nielsen, S. B. (2017). Nucleation process of magnitude 2 repeating earthquakes on the San Andreas Fault predicted by rate-and-state fault models with SAFOD drill core data. *Geophysical Research Letters*, *44*(1), 162–173. https://doi.org/10.1002/2016gl071569

Kaneko, Y., Nielsen, S. B., & Carpenter, B. M. (2016). The onset of laboratory earthquakes explained by nucleating rupture on a rate-and-state fault. *Journal of Geophysical Research: Solid Earth*, *121*(8), 6071–6091. https://doi.org/10.1002/2016jb013143

Kaneko, Y., Sims, N. E., Holtkamp, S. G., & Tape, C. (2019). Accelerating foreshocks of crustal earthquakes controlled by frictional heterogeneities. *AGU Fall Meeting Abstracts*, *2019*, S21F–0571.

Kato, A., Obara, K., Igarashi, T., Tsuruoka, H., Nakagawa, S., & Hirata, N. (2012). Propagation of slow slip leading up to the 2011 M w 9.0 Tohoku-Oki earthquake. *Science*, *335*(6069), 705–708. https://doi.org/10.1126/science.1215141

Latour, S., Schubnel, A., Nielsen, S., Madariaga, R., & Vinciguerra, S. (2013). Characterization of nucleation during laboratory earthquakes. *Geophysical Research Letters*, *40*(19), 5064–5069. https://doi.org/10.1002/grl.50974

Liu, Y., & Rice, J. R. (2005). Aseismic slip transients emerge spontaneously in three-dimensional rate and state modeling of subduction earthquake sequences. *Journal of Geophysical Research*, *110*(B8). https://doi.org/10.1029/2004jb003424

Luo, Y., & Ampuero, J. P. (2018). Stability of faults with heterogeneous friction properties and effective normal stress. *Tectonophysics*, *733*, 257–272. https://doi.org/10.1016/j.tecto.2017.11.006

Martínez-Garzón, P., & Poli, P. (2024). Cascade and pre-slip models oversimplify the complexity of earthquake preparation in nature. *Communications Earth & Environment*, *5*(1), 120. https://doi.org/10.1038/s43247-024-01285-y

McLaskey, G. C. (2019). Earthquake initiation from laboratory observations and implications for foreshocks. *Journal of Geophysical Research: Solid Earth*, *124*(12), 12882–12904. https://doi.org/10.1029/2019jb018363

McLaskey, G. C., & Lockner, D. A. (2014). Preslip and cascade processes initiating laboratory stick slip. *Journal of Geophysical Research: Solid Earth*, *119*(8), 6323–6336. https://doi.org/10.1002/2014jb011220

Meng, L., Huang, H., Bürgmann, R., Ampuero, J. P., & Strader, A. (2015). Dual megathrust slip behaviors of the 2014 Iquique earthquake sequence. *Earth and Planetary Science Letters*, *411*, 177–187. https://doi.org/10.1016/j.epsl.2014.11.041

Mignan, A. (2014). The debate on the prognostic value of earthquake foreshocks: A meta-analysis. *Scientific Reports*, *4*(1), 4099. https://doi.org/10.1038/srep04099

Mogi, K. (1963). Some discussions on aftershocks, foreshocks and earthquake swarms-the fracture of a semi finite body caused by an inner stress origin and its relation to the earthquake phenomena. *Bulletin of the Earthquake Research Institute*, *41*, 615–658.

Nishikawa, T., Ide, S., & Nishimura, T. (2023). A review on slow earthquakes in the Japan Trench. *Progress in Earth and Planetary Science*, *10*(1), 1–51. https://doi.org/10.1186/s40645-022-00528-w

Obara, K. (2002). Nonvolcanic deep tremor associated with subduction in southwest Japan. *Science*, *296*(5573), 1679–1681. https://doi.org/10.1126/science.1070378

Obara, K., & Kato, A. (2016). Connecting slow earthquakes to huge earthquakes. *Science*, *353*(6296), 253–257. https://doi.org/10.1126/science.aaf1512

Ohnaka, M., & Shen, L. F. (1999). Scaling of the shear rupture process from nucleation to dynamic propagation: Implications of geometric irregularity of the rupturing surfaces. *Journal of Geophysical Research*, *104*(B1), 817–844. https://doi.org/10.1029/1998jb900007

Okuda, T., & Ide, S. (2018). Hierarchical rupture growth evidenced by the initial seismic waveforms. *Nature Communications*, *9*(1), 3714. https://doi.org/10.1038/s41467-018-06168-3

Omori, F. (1894). *On the aftershocks of earthquakes* (Vol. 7, pp. 111–120). Imperial University of Tokyo.

Passelègue, F. X., Latour, S., Schubnel, A., Nielsen, S., Bhat, H. S., & Madariaga, R. (2017). Influence of fault strength on precursory processes during laboratory earthquakes. *Fault zone dynamic processes: Evolution of fault properties during seismic rupture*, 229–242.

Peng, Z., & Lei, X. (2024). Physical mechanisms of earthquake nucleation and foreshocks: Cascade triggering, aseismic slip, or fluid flows? *Earthquake Research Advances*, *5*(2), 100349. https://doi.org/10.1016/j.eqrea.2024.100349

Radiguet, M., Perfettini, H., Cotte, N., Gualandi, A., Valette, B., Kostoglodov, V., et al. (2016). Triggering of the 2014 M w 7.3 Papanoa earthquake by a slow slip event in Guerrero, Mexico. *Nature Geoscience*, *9*(11), 829–833. https://doi.org/10.1038/ngeo2817

Ross, Z. E., Hauksson, E., & Ben-Zion, Y. (2017). Abundant off-fault seismicity and orthogonal structures in the San Jacinto fault zone. *Science Advances*, *3*(3), e1601946. https://doi.org/10.1126/sciadv.1601946

Rubin, A. M. (2008). Episodic slow slip events and rate-and-state friction. *Journal of Geophysical Research*, *113*(B11). https://doi.org/10.1029/2008jb005642

Rubin, A. M., & Ampuero, J. P. (2005). Earthquake nucleation on (aging) rate and state faults. *Journal of Geophysical Research*, *110*(B11). https://doi.org/10.1029/2005jb003686

Scholz, C. H. (1998). Earthquakes and friction laws. *Nature*, *391*(6662), 37–42. https://doi.org/10.1038/34097

Shaddox, H. R., Schwartz, S. Y., & Bartlow, N. M. (2021). Afterslip and spontaneous aseismic slip on the Anza segment of the San Jacinto Fault Zone, Southern California. *Journal of Geophysical Research: Solid Earth*, *126*(6), e2020JB020460. https://doi.org/10.1029/2020jb020460

Shearer, P. M., Meng, H., & Fan, W. (2023). Earthquake detection using a nodal array on the San Jacinto fault in California: Evidence for high foreshock rates preceding many events. *Journal of Geophysical Research: Solid Earth*, *128*(3), e2022JB025279. https://doi.org/10.1029/2022jb025279

Shelly, D. R. (2017). A 15 year catalog of more than 1 million low-frequency earthquakes: Tracking tremor and slip along the deep San Andreas Fault. *Journal of Geophysical Research: Solid Earth*, *122*(5), 3739–3753. https://doi.org/10.1002/2017jb014047

Shelly, D. R., Beroza, G. C., & Ide, S. (2007). Non-volcanic tremor and low-frequency earthquake swarms. *Nature*, *446*(7133), 305–307. https://doi.org/10.1038/nature05666

Skarbek, R. M., Rempel, A. W., & Schmidt, D. A. (2012). Geologic heterogeneity can produce aseismic slip transients. *Geophysical Research Letters*, *39*(21). https://doi.org/10.1029/2012gl053762

Socquet, A., Valdes, J. P., Jara, J., Cotton, F., Walpersdorf, A., Cotte, N., et al. (2017). An 8 month slow slip event triggers progressive nucleation of the 2014 Chile megathrust. *Geophysical Research Letters*, *44*(9), 4046–4053. https://doi.org/10.1002/2017gl073023

Tape, C., Holtkamp, S., Silwal, V., Hawthorne, J., Kaneko, Y., Ampuero, J. P., et al. (2018). Earthquake nucleation and fault slip complexity in the lower crust of central Alaska. *Nature Geoscience*, *11*(7), 536–541. https://doi.org/10.1038/s41561-018-0144-2

Uchida, N., Matsuzawa, T., Ellsworth, W. L., Imanishi, K., Shimamura, K., & Hasegawa, A. (2012). Source parameters of microearthquakes on an interplate asperity off Kamaishi, NE Japan over two earthquake cycles. *Geophysical Journal International*, *189*(2), 999–1014. https://doi.org/10.1111/j.1365-246x.2012.05377.x

U.S. Geological Survey. (1931). United States national strong-motion network [Dataset]. *International Federation of Digital Seismograph Networks*. https://doi.org/10.7914/SN/NP

Wang, J., Templeton, D. C., & Harris, D. B. (2015). Discovering new events beyond the catalogue—application of empirical matched field processing to Salton Sea geothermal field seismicity. *Geophysical Journal International*, *203*(1), 22–32. https://doi.org/10.1093/gji/ggv260

Wdowinski, S. (2009). Deep creep as a cause for the excess seismicity along the San Jacinto fault. *Nature Geoscience*, *2*(12), 882–885. https://doi.org/10.1038/ngeo684

Yamashita, F., Fukuyama, E., Xu, S., Kawakata, H., Mizoguchi, K., & Takizawa, S. (2021). Two end-member earthquake preparations illuminated by foreshock activity on a meter-scale laboratory fault. *Nature Communications*, *12*(1), 4302. https://doi.org/10.1038/s41467-021-24625-4

Yoshida, S., & Ogawa, T. (2004). Electromagnetic emissions from dry and wet granite associated with acoustic emissions. *Journal of Geophysical Research*, *109*(B9). https://doi.org/10.1029/2004jb003092

References From the Supporting Information

Huang, H., Xu, W., Meng, L., Bürgmann, R., & Baez, J. C. (2017). Early aftershocks and afterslip surrounding the 2015 Mw 8.4 Illapel rupture. *Earth and Planetary Science Letters*, *457*, 282–291. https://doi.org/10.1016/j.epsl.2016.09.055

Hutton, K., Woessner, J., & Hauksson, E. (2010). Earthquake monitoring in southern California for seventy-seven years (1932–2008). *Bulletin of the Seismological Society of America*, *100*(2), 423–446. https://doi.org/10.1785/0120090130

Mordret, A., Brenguier, F., Causse, M., Boué, P., Voisin, C., Dumont, I., et al. (2020). Seismic stereometry reveals preparatory behavior and source kinematics of intermediate-size earthquakes. *Geophysical Research Letters*, *47*(17), e2020GL088563. https://doi.org/10.1029/2020gl088563

Zhang, M., & Wen, L. (2015). An effective method for small event detection: Match and locate (M&L). *Geophysical Journal International*, *200*(3), 1523–1537.